



## Full Length Article

# Solid solution structural engineering enhances the luminescence of SrMgAl<sub>10</sub>O<sub>17</sub>:Cr<sup>3+</sup> for agricultural lighting

Yibiao Ma<sup>a,b</sup>, Weifang Liao<sup>a,b</sup>, Beibei Quan<sup>a,b</sup>, Zihui Kong<sup>a</sup>, Maxim S. Molokeev<sup>c</sup>, Andrey Zolotov<sup>c</sup>, Ming Cheng<sup>d</sup>, Xiaoyan Chen<sup>d</sup>, Zhi Zhou<sup>a,b,\*\*</sup>, Mao Xia<sup>a,b,\*</sup>

<sup>a</sup> School of Chemistry and Materials Science, Hunan Agricultural University, Changsha 410128, PR China

<sup>b</sup> Hunan Optical Agriculture Engineering Technology Research Center, Changsha 410128, PR China

<sup>c</sup> World-Class Research Center "Advanced Digital Technologies", University of Tyumen, Tyumen 625003, Russia

<sup>d</sup> Dongguan Ledstar Optoelectronics Technology Co., Ltd, Dongguan, 523000, PR China

## ARTICLE INFO

## Keywords:

Optical material  
Indoor plant cultivation  
Far-red light  
SrMgAl<sub>10</sub>O<sub>17</sub>

## ABSTRACT

Lead-free non-rare earth oxide phosphors have attracted wide attention due to their environmental protection, sustainability, and potential to replace halides and fluorides in the field of plant lighting. Among them, the Cr<sup>3+</sup>-excited aluminate phosphor exhibits high brightness, high thermal stability, and far red to near-infrared (NIR) emission due to the influence of the crystal field strength (CFS). This property gives rise to a variety of strategies used to modulate the CFS, for example, single ion substitution, chemical unit co-substitution, etc. Here, we chose the substitution of a single ion, with [BaO<sub>6</sub>] gradually replacing [SrO<sub>6</sub>] to form a solid solution. Their structural characteristics and the local structure of Cr<sup>3+</sup> are studied and discussed. The device is packaged to evaluate the feasibility of the material for practical application. The prepared phosphor had a bright far-red light emission of 693 nm under blue light excitation, and this spectrum strongly matched the absorption of plant phytochrome P<sub>FR</sub>. This work provides the design principle of far red light emission activated by Cr<sup>3+</sup> aluminate solid solution, which can inspire further research on pc-LED lights for plant lighting.

## 1. Introduction

With the improvement of people's living standards and the rapid development of industrialization, global resources have been over-exploited, which has seriously affected the ecological environment [1, 2]. Furthermore, extreme weather, serious water pollution, and air pollution have made it impossible for traditional agricultural production methods better to meet the supply and demand in today's society. Using modern engineering technology, indoor plant cultivation (IPC) makes the growth of crops no longer subject to the external natural ecological environment, greatly improves the crop's production efficiency, and brings more economic and social benefits [3–7]. Light is a necessary environmental condition for plant growth, which has important effects on biological phenomena such as photosynthesis, color development, phototropism, and morphogenesis of plants. Phytochrome P<sub>R</sub> and Phytochrome P<sub>FR</sub> are distributed in various plant organs, mainly absorbing red light (600–680 nm) and far-red light (680–780 nm), of which far-red light can promote the formation of chlorophyll and

carbohydrates, affecting plant flowering, stem elongation, and seed germination [8–14]. Phosphors-converted light-emitting diodes (pc-LEDs) are the inevitable trend of scientific and technological development to replace the traditional light source. Pc-LEDs have become the main light source for ICP due to their advantages of energy-saving, environment-friendly, long life, and high efficiency [15, 16]. At present, a large number of reports of red phosphors are mainly based on luminescent materials activated by rare earth ions. For example, CaAlSiN<sub>3</sub>:Eu<sup>2+</sup>, Ca<sub>2</sub>BO<sub>3</sub>Cl: Sm<sup>3+</sup>, and Cs<sub>2</sub>NaBiCl<sub>6</sub>: Mn<sup>2+</sup> [17–20]. However, these phosphors are not suitable for agricultural lighting due to the presence of toxic substances, high prices, harsh synthesis conditions and other shortcomings. Therefore, a new type of environmentally friendly, low-cost, and easy-to-synthesize far-red phosphor has been developed.

Cr<sup>3+</sup>, virtually nontoxic and inexpensive, is the ideal emission center for red/far red light. The luminous characteristics of Cr<sup>3+</sup> are greatly affected by the crystal field environment, and the <sup>2</sup>E → <sup>4</sup>A<sub>2</sub> transition of the outermost 3d<sup>3</sup> energy layer can exhibit far-red luminescence

\* Corresponding author. School of Chemistry and Materials Science, Hunan Agricultural University, Changsha 410128, PR China.

\*\* Corresponding author. School of Chemistry and Materials Science, Hunan Agricultural University, Changsha 410128, PR China.

E-mail addresses: [zhouzhi@hunau.edu.cn](mailto:zhouzhi@hunau.edu.cn) (Z. Zhou), [xiamao2014@163.com](mailto:xiamao2014@163.com) (M. Xia).

[21–24]. The excitation range of  $\text{Cr}^{3+}$  is 250 nm–650 nm, and there are generally three excitation peaks, among which the excitation peak located in the blue light range can well match the commercial blue light chip. Such  $\text{Cr}^{3+}$  activated phosphor such as  $\text{ZnGa}_2\text{O}_4:\text{Cr}^{3+}$  and  $\text{LiGa}_5\text{O}_8:\text{Cr}^{3+}$  have good performance [25–28]. Against  $\text{Cr}^{3+}$ -activated aluminate phosphors, also previously reported, for example,  $\text{ZnAl}_2\text{O}_4:\text{Cr}^{3+}$  has multi-peak broadband emissions [29,30].

Both  $\text{SrMgAl}_{10}\text{O}_{17}$  and  $\text{BaMgAl}_{10}\text{O}_{17}$  belong to the hexagonal crystal system and have the same  $\beta$ -alumina type with space group  $P63/mmc$  [31–33].  $\text{Cr}^{3+}$  has the same valence state, similar ion radius, and electronegativity as  $\text{Al}^{3+}$ , so  $\text{Cr}^{3+}$  easily replaces  $\text{Al}^{3+}$  into the host lattice and occupies the octahedral site, resulting in red and far red radiation transitions. According to our understanding, although there are reports on  $\text{Cr}^{3+}$  doped  $\text{SrMgAl}_{10}\text{O}_{17}$  or  $\text{BaMgAl}_{10}\text{O}_{17}$ , so far, there have been no reports on the luminescence properties of  $\text{Cr}^{3+}$  in the orthogonal  $\text{Sr}_{1-y}\text{Ba}_y\text{MgAl}_{10}\text{O}_{17}$  solid solution. In this work, we focused on the crystal structure of the  $\text{Cr}^{3+}$ -doped  $\text{Sr}_{1-y}\text{Ba}_y\text{MgAl}_{10}\text{O}_{17}$  solid solution and improved thermal stability, luminous intensity, and quantum efficiency of the luminescent material. The optimal performance of the material is prepared as an LED device combined with a blue light chip, showing a mixture of bright blue and red light, matching the plant pigment absorption spectrum, indicating that this phosphor is suitable as a light source for indoor plant cultivation.

## 2. Experimental sections

### 2.1. Materials and synthesis

The  $\text{SrMgAl}_{10}\text{O}_{17}:\text{xCr}^{3+}$  ( $x = 0.005, 0.01, 0.015, 0.02, 0.025$ ) and  $\text{Sr}_{1-y}\text{Ba}_y\text{MgAl}_{10}\text{O}_{17}:\text{Cr}^{3+}$  ( $y = 0, 0.2, 0.4, 0.6, 0.8, 1.0$ ) phosphors were prepared by high-temperature solid-state reaction. Analytical-grade reagents  $\text{SrCO}_3$  (99.99%),  $\text{BaCO}_3$  (99.99%),  $\text{MgO}$  (99.99%),  $\text{Al}_2\text{O}_3$  (99.99%),  $\text{Cr}_2\text{O}_3$  (99.99%) were used as raw materials, which purchased from Aladdin. According to the stoichiometric ratio, they were weighting the starting materials and adding a mass fraction of 2 % wt  $\text{H}_3\text{BO}_3$  as cosolvent. Subsequently, the mixtures were placed in an agate mortar with a few drops of alcohol and grinded carefully for 30 min. Then the mixed samples were loaded into the crucible, and sintered at 1300 °C for 6 h in a high-temperature furnace. Ultimately, these samples were cooled to room temperature naturally for grinding for subsequent tests.

### 2.2. Measurements and characterization

The X-ray diffraction (XRD) data of these phosphors were measured by an X-ray diffractometer (PANalytical, Netherlands). The scanning range was from 10° to 120°, and the scanning rate was 10°/min. Excitation and emission spectra were measured by a F-4700 spectrometer (Hitachi, Japan), excited by 150 W Xe lamp. The thermal stability of phosphors was tested by controlling their temperature with a heat controller (Orient KOJI, China). The surface topography of the samples was recorded by dual-beam scanning electron microscope (SEM) microscope (FEI helios nanolab G3 UC, USA), and elemental analysis was recorded by energy dispersive X-ray detector (EDX). The internal quantum efficiency (IQE) was collected using a QE-2100 test system (Otsuka, Japan). The UV–disuse reflection spectroscopy was recorded by a UV-2600i spectrophotometer (Shimadzu, Japan).

## 3. Results and discussion

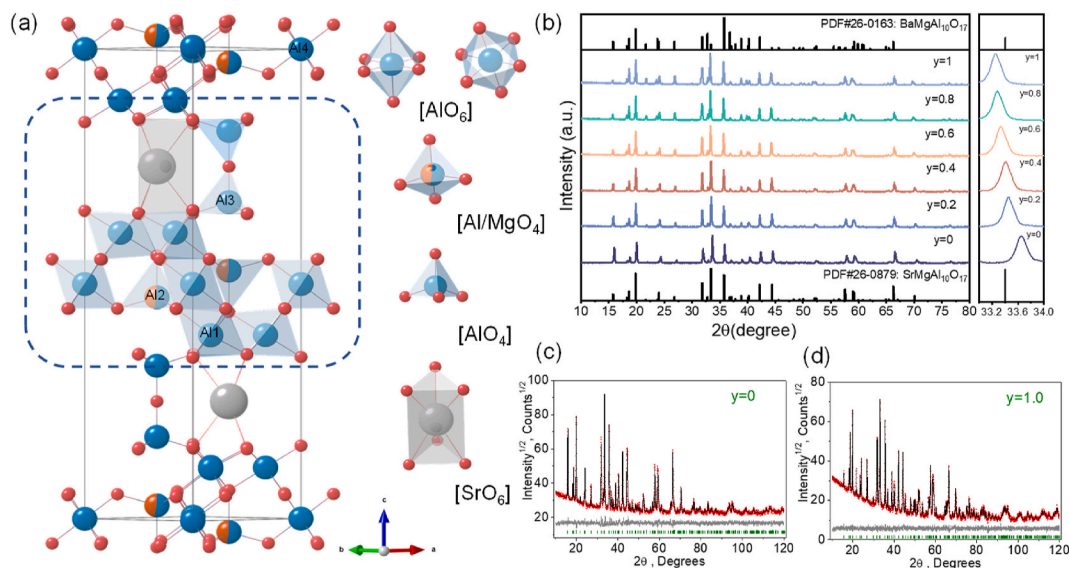
### 3.1. Crystal structure and morphological characterization

Fig. 1a shows the  $\text{SrMgAl}_{10}\text{O}_{17}$  crystal structure model, belonging to the hexagonal system,  $P63/mmc$  space group,  $\text{Al}^{3+}$  occupy four different sites, labeled Al1, Al2, Al3, Al4, for more information included in Table 1 and Tabs1-S3. Four different Al sites respectively belong to two octahedrons [ $\text{AlO}_6$ ] and two kinds of tetrahedral [ $\text{AlO}_4$ ]. When  $\text{Cr}^{3+}$  ion doping, due to the ionic radius of  $\text{Cr}^{3+}$  ion (CN = 6,  $r = 0.62 \text{ \AA}$ ) and the ionic radius of  $\text{Al}^{3+}$  ion (CN = 6,  $r = 0.54 \text{ \AA}$ ) are similar, and  $\text{Cr}^{3+}$  ion tends to occupy the octahedral position site, thus  $\text{Cr}^{3+}$  ion will replace the Al4 and Al1 site.  $\text{Sr}^{2+}$  ion forms a hexahedron [ $\text{SrO}_6$ ] with six adjacent oxygen atoms. It is adjacent to the octahedron where Al1 is located, which means that the change of [ $\text{SrO}_6$ ] is likely to cause a change in the environment of the Al1 site. In other words, it may change

**Table 1**

The coordination environment information of  $\text{Al}^{3+}$  ions in  $\text{SrMgAl}_{10}\text{O}_{17}$ .

Atom	x	y	z	$B_{\text{iso}}$	Occ.
Al1	0.8360(3)	0.6720(5)	0.10728(11)	0.39(18)	1
Al2	0.3333333	0.6666667	0.02407(18)	0.2(2)	0.5
Al3	0.3333333	0.6666667	0.1739(2)	0.4(2)	1
Al4	0	0	0	0.7(2)	1



**Fig. 1.** (a) Schematic representation of the structure of the  $\text{SrMgAl}_{10}\text{O}_{17}$  matrix; (b) The XRD pattern of  $\text{Sr}_{1-y}\text{Ba}_y\text{MgAl}_{10}\text{O}_{17}:\text{Cr}^{3+}$  ( $y = 0-1$ ); (c) and (d) XRD refinements of  $\text{SrMgAl}_{10}\text{O}_{17}:\text{Cr}^{3+}$  and  $\text{BaMgAl}_{10}\text{O}_{17}:\text{Cr}^{3+}$ .

the crystal field environment of the  $\text{Cr}^{3+}$  ion and then regulate the luminescence of the  $\text{Cr}^{3+}$  ion. Fig. 1b shows the XRD pattern of  $\text{Ba}^{2+}$  ion gradually replacing  $\text{Sr}^{2+}$  ion. When  $y = 0$  and  $y = 1$ , samples of diffraction peak corresponding to the perfect  $\text{SrMgAl}_{10}\text{O}_{17}$  (PDF# 26-0879) and  $\text{BaMgAl}_{10}\text{O}_{17}$  card (PDF# 26-0163), and refinement results also prove that there are no other impurities (Fig. S1).  $\text{Ba}^{2+}$  ion radius (CN = 6,  $r = 0.135 \text{ \AA}$ ) is greater than the  $\text{Sr}^{2+}$  ion (CN = 6,  $r = 0.118 \text{ \AA}$ ), according to Bragg's law:  $2d\sin\theta = n\lambda$ , the displacement of small radius ions by large radius ions leads to a shift of diffraction peak to a lower angle. This phenomenon is observed in the inset of Fig. 1b. The refinement results for  $y = 0.2\text{--}0.8$  samples are included in, Fig. S1 and the linear increase in unit cell volume indicates successful sample preparation.

Fig. 2a indicates a SEM image  $\text{Sr}_{0.2}\text{Ba}_{0.8}\text{MgAl}_{10}\text{O}_{17}:0.02\text{Cr}^{3+}$  phosphor. It shows that the particle is a smooth-surfaced polyhedron, and the particle size is about  $15 \mu\text{m}$ , with good crystallinity and a clear grain boundary. Fig. 2b is an element map of the selected sample, and corresponding spectral energy distribution (EDS) which shows the element distribution of Sr, Ba, Mg, Al, O, and Cr.  $\text{Cr}^{3+}$  has been successfully incorporated into  $\text{Sr}_{0.2}\text{Ba}_{0.8}\text{MgAl}_{10}\text{O}_{17}$  crystal structure, which can be reflected from the uniform distribution of various elements, and the ideal phosphor has been successfully synthesized.

### 3.2. Photoluminescent properties

In previous reports on  $\text{Sr}/\text{BaMgAl}_{10}\text{O}_{17}:\text{Cr}^{3+}$ , it has been learned that the emission spectrum of  $\text{Sr}/\text{BaMgAl}_{10}\text{O}_{17}:\text{Cr}^{3+}$  is strictly dependent on the concentration of  $\text{Cr}^{3+}$  ion: at low concentrations, narrow-band emission around  $693 \text{ nm}$  dominates, whereas at high concentrations, broadband emission attributed to  ${}^4\text{T}_2 \rightarrow {}^4\text{A}_2$  dominates. In this work, our research focuses on far-red light emission at  $693 \text{ nm}$ . Fig. 3a shows the emission spectrum of  $\text{SrMgAl}_{10}\text{O}_{17}$  at different  $\text{Cr}^{3+}$  concentrations, with the increase of  $\text{Cr}^{3+}$  concentration, the emission intensity of  $\text{SrMgAl}_{10}\text{O}_{17}$  gradually increases. When  $x = 0.02$ , it reaches the peak. Therefore, the sample with a concentration of  $\text{Cr}^{3+} = 0.02$  was selected in the subsequent substitution project. In Fig. 3b, the excitation

spectrum of the  $\text{Cr}^{3+}$  ion covers the range from  $300 \text{ nm}$  to  $650 \text{ nm}$ . It is divided into two parts: the spin-allowed transition from the  ${}^4\text{A}_2 \rightarrow {}^4\text{T}_1$  energy level and the transition from the  ${}^4\text{A}_2 \rightarrow {}^4\text{T}_2$  energy level, corresponding to peak positions of  $399 \text{ nm}$  and  $554 \text{ nm}$ , respectively [34–37]. The emission peak of  $\text{SrMgAl}_{10}\text{O}_{17}$  comes from the  ${}^2\text{E} \rightarrow {}^4\text{A}_2$  energy level transition (Fig. 3c), covering a range of  $650 \text{ nm--}800 \text{ nm}$ , with a peak of  $693 \text{ nm}$ . A schematic representation of the  $\text{Cr}^{3+}$  electron being excited to produce a transition is depicted. In  $\text{SrMgAl}_{10}\text{O}_{17}:\text{Cr}^{3+}$ , electrons are excited to produce three different transitions (Fig. 3d), the  ${}^4\text{A}_2 \rightarrow {}^4\text{T}_1$  ( ${}^4\text{P}$ ) transition can be observed in the excitation peak of  $200 \text{ nm--}300 \text{ nm}$ , but the spectrum of excitation shows that the probability of this transition occurring is weak, and more excitation comes from  ${}^4\text{A}_2 \rightarrow {}^4\text{T}_1$  ( ${}^4\text{P}$ ) and  ${}^4\text{A}_2 \rightarrow {}^4\text{T}_2$ . Although the intensity from the  ${}^4\text{A}_2 \rightarrow {}^4\text{T}_2$  transition is almost close to that of  ${}^4\text{A}_2 \rightarrow {}^4\text{T}_1$  ( ${}^4\text{F}$ ), considered a more convenient commercial blue-light chip, this work focuses on the excitation peak at  $399 \text{ nm}$ .

The far-red emission of  $\text{Cr}^{3+}$  is most likely due to the strong crystal field environment. Introduce the Racah parameter and use the following equation for the calculation [38,39]:

$$10Dq = E({}^4T_2) = E({}^4A_2 \rightarrow {}^4T_2) - \Delta S/2 \quad (1)$$

$$\frac{B}{Dq} = \frac{\left(\frac{\Delta E_{4T}}{Dq}\right)^2 - 10\left(\frac{\Delta E_{4T}}{Dq}\right)}{15\left(\frac{\Delta E_{4T}}{Dq} - 8\right)} \quad (2)$$

$$\Delta E_{4T} = E({}^4T_1) - E({}^4T_2) \quad (3)$$

$$\beta_1 = \sqrt{\left(\frac{B}{B_0}\right)^2 + \left(\frac{C}{C_0}\right)^2} \quad (4)$$

The calculated  $Dq/B$  value is  $2.46$  (Fig. 3e), which is not equal to but greater than  $2.3$ , indicating that  $\text{Cr}^{3+}$  is in a strong crystal field, corresponding to the far-red light emission emitted by this material.

The triangular prismatic site occupied by  $\text{Sr}^{2+}$  ion in SMAO shares O atoms with the octa-planar position site occupied by  $\text{Al}^{3+}$  ion. When

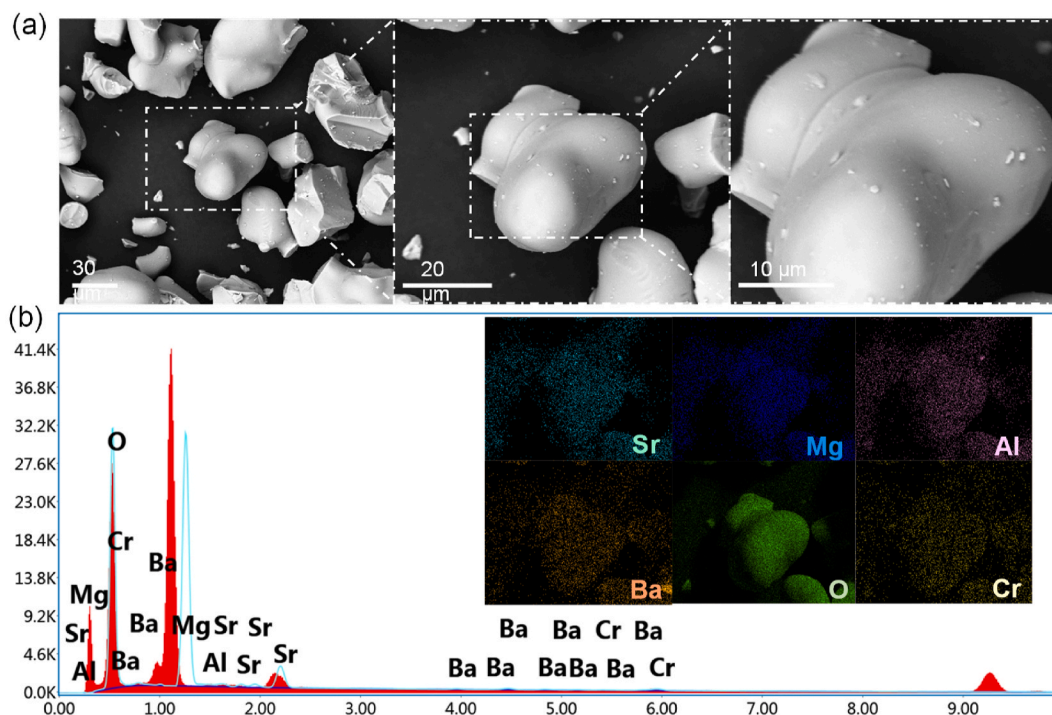
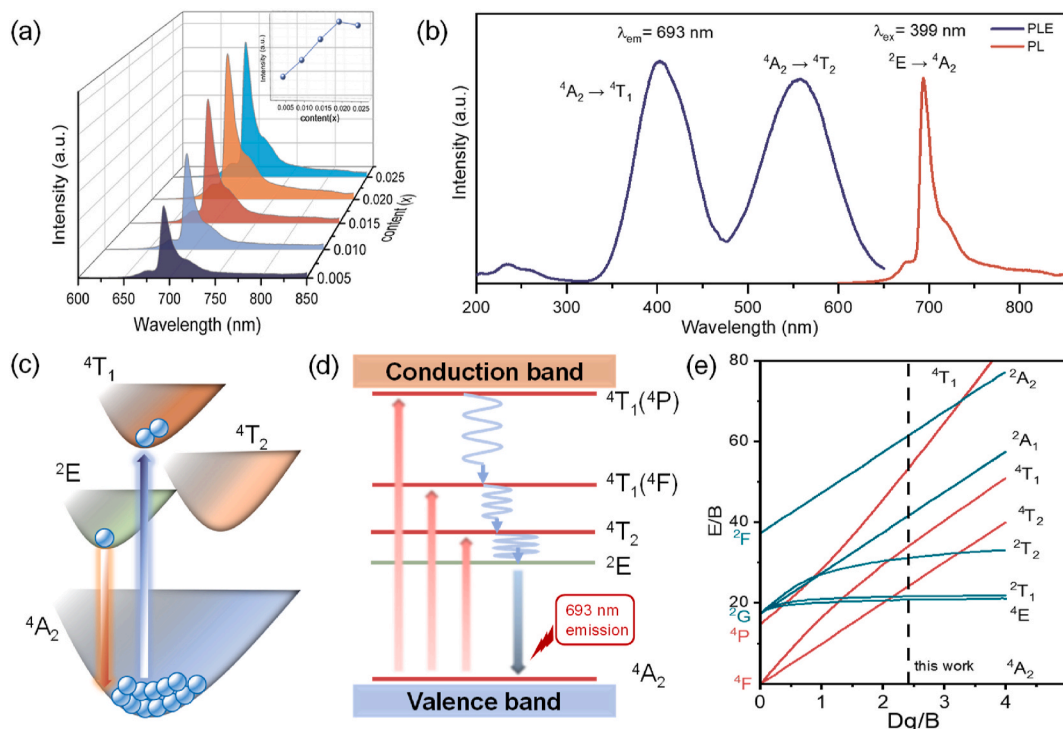


Fig. 2. (a) SEM images of  $\text{Sr}_{0.2}\text{Ba}_{0.8}\text{MgAl}_{10}\text{O}_{17}:0.02\text{Cr}^{3+}$  phosphor in various detecting scales; (b) EDS spectra of selected  $\text{Sr}_{0.2}\text{Ba}_{0.8}\text{MgAl}_{10}\text{O}_{17}:0.02\text{Cr}^{3+}$  particle and the corresponding elemental mapping images for Sr, Ba, Mg, Al, O, and Cr in  $\text{Sr}_{0.2}\text{Ba}_{0.8}\text{MgAl}_{10}\text{O}_{17}:0.02\text{Cr}^{3+}$ .



**Fig. 3.** (a) Emission spectra of  $\text{SrMgAl}_{10}\text{O}_{17}: x\text{Cr}^{3+}$ ; (b) Excitation and emission spectra of  $\text{SrMgAl}_{10}\text{O}_{17}: 0.02\text{Cr}^{3+}$ ; (c) and (d)  $\text{Cr}^{3+}$  electron transition diagram and radiation transition diagram; (e) Tanabe-Sugano diagram for the  $d^3$  electronic configuration in an octahedral symmetry.

$\text{Sr}^{2+}$  ion is gradually replaced by  $\text{Ba}^{2+}$  ion, the luminescence of SMAO is greatly enhanced (Fig. 4a b), while spectral broadening is observed in the normalized figure (Fig. 4c). When  $y = 0.8$ , the highest point is reached, and the integrated intensity increases to 254 % of the initial strength. This is caused by a change in the strength of the crystal field in which  $\text{Cr}^{3+}$  is located. The  $Dq/B$  values for  $y = 0-1$  were also calculated

and are listed in Table S4. The gradually increasing  $\text{Ba}^{2+}$  ions lead to an enhanced lattice distortion, which in turn leads to an enhanced crystal field strength, while when  $y = 1$ , the material undergoes a fundamental change, reaching a new equilibrium and, as a result, the CFS decreases. The increase in crystal field strength leads to a more intense far-red emission of  $\text{Cr}^{3+}$ , before which far red emission of  $\text{Cr}^{3+}$  is significantly

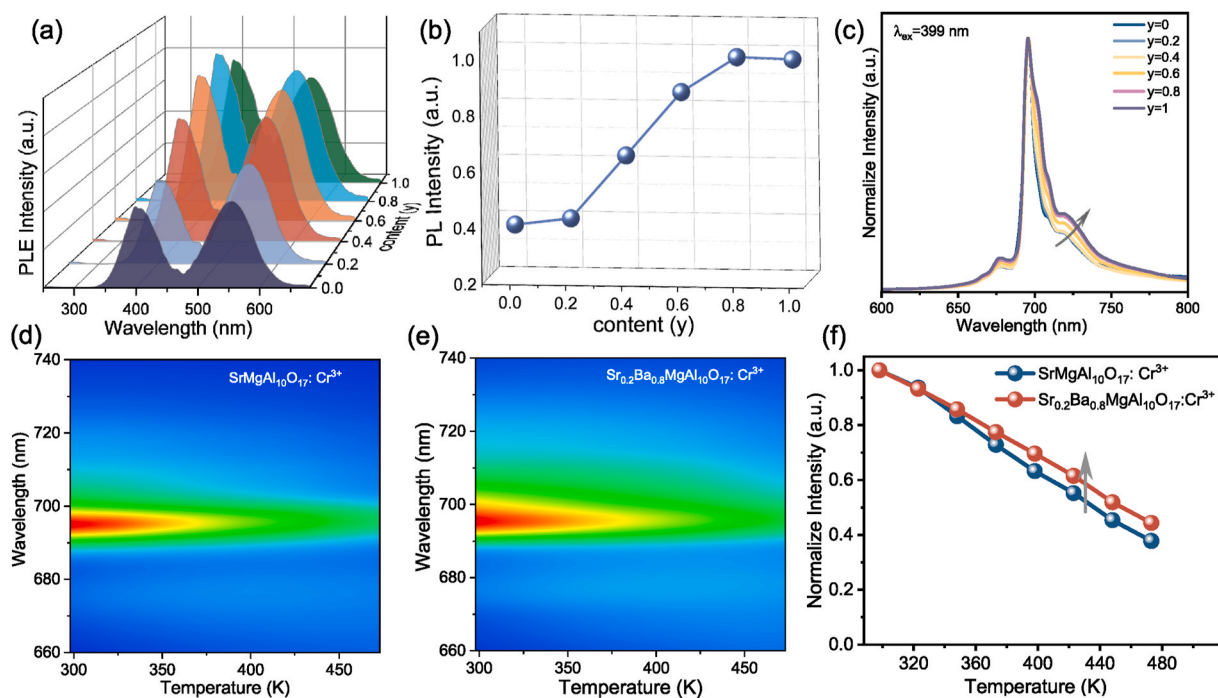


**Fig. 4.** (a) Excitation spectrum of  $\text{Sr}_{1-y}\text{Ba}_y\text{MgAl}_{10}\text{O}_{17}: \text{Cr}^{3+}$  ( $y = 0-1$ ); (b) The integrated intensity of  $\text{Sr}_{1-y}\text{Ba}_y\text{MgAl}_{10}\text{O}_{17}: \text{Cr}^{3+}$  ( $y = 0-1$ ) emission; (c) Normalized emission spectra; (d) and (e) temperature dependence spectra of  $\text{SrMgAl}_{10}\text{O}_{17}: \text{Cr}^{3+}$  and  $\text{Sr}_{0.2}\text{Ba}_{0.8}\text{MgAl}_{10}\text{O}_{17}: \text{Cr}^{3+}$  ( $y = 0-1$ ) from 298 K to 473 K; (f) normalized spectra of two phosphors.

enhanced.

An important indicator to evaluate the application prospects of phosphors is their stability at high temperatures. The temperature-dependent emission spectra of  $\text{SrMgAl}_{10}\text{O}_{17}:\text{Cr}^{3+}$  and  $\text{Sr}_{0.2}\text{Ba}_{0.8}\text{MgAl}_{10}\text{O}_{17}:\text{Cr}^{3+}$  were tested, and as shown in Fig. 4d and e, the luminescence intensity of both samples showed a sharp decrease with increasing temperature, maintaining 55.2 % and 61.5 % of that at room temperature at 423 K, respectively. The thermal stability of samples substituted with  $\text{Ba}^{2+}$  ions showed a slight enhancement. Generally speaking, the  $\text{Cr}^{3+}$ -activated phosphors will be subjected to severe thermal quenching, resulting in a decrease in luminous intensity. A material with good thermal stability generally has one or more characteristics: i) strong structural rigidity; and ii) a large band gap [40]. In SMAO, the strong thermal quenching occurs due to the nonradiative transition of thermally excited electrons back to the ground state through the intersection of  ${}^4\text{A}_2$  and  ${}^4\text{T}_2$ . The difficulty of reaching the intersection depends on the thermal activation energy ( $E_a$ ). It is calculated by the following formula [7,41,42]:

$$I(T) = \frac{I_0}{1 + c \exp\left(\frac{-E_a}{kT}\right)} \quad (4)$$

where  $I(T)$  and  $I_0$  are integrated PL intensity at a given temperature and initial temperature,  $k$  is a Boltzmann constant ( $8.617 \times 10^{-5}$  eV/K), and  $c$  is a constant that is related to the matrix. The  $E_a$  values of  $\text{SrMgAl}_{10}\text{O}_{17}:\text{Cr}^{3+}$  and  $\text{Sr}_{0.2}\text{Ba}_{0.8}\text{MgAl}_{10}\text{O}_{17}:\text{Cr}^{3+}$  were 0.26 eV and 0.24 eV, respectively (Fig. S2).

Fig. 5a tests the UV diffuse reflectance spectrum of  $\text{Sr}_{1-y}\text{Ba}_y\text{MgAl}_{10}\text{O}_{17}:\text{Cr}^{3+}$  ( $y = 0, 0.2, 0.4, 0.6, 0.8, 1.0$ ) and the host. SMAO is a flat plot line without any absorption. There are three absorption bands in the spectrum were observed, which are weak absorption bands between 200 nm and 230 nm, a strong absorption band from 320 nm to 470 nm, and an absorption band from 500 nm to 620 nm, respectively. Corresponding to the excitation spectrum of  $\text{Cr}^{3+}$ . The optical band gap can be calculated according to the following formula [43,44]:

$$F(R_\infty) = (1 - R_\infty)^2 / (2R_\infty) \quad (5)$$

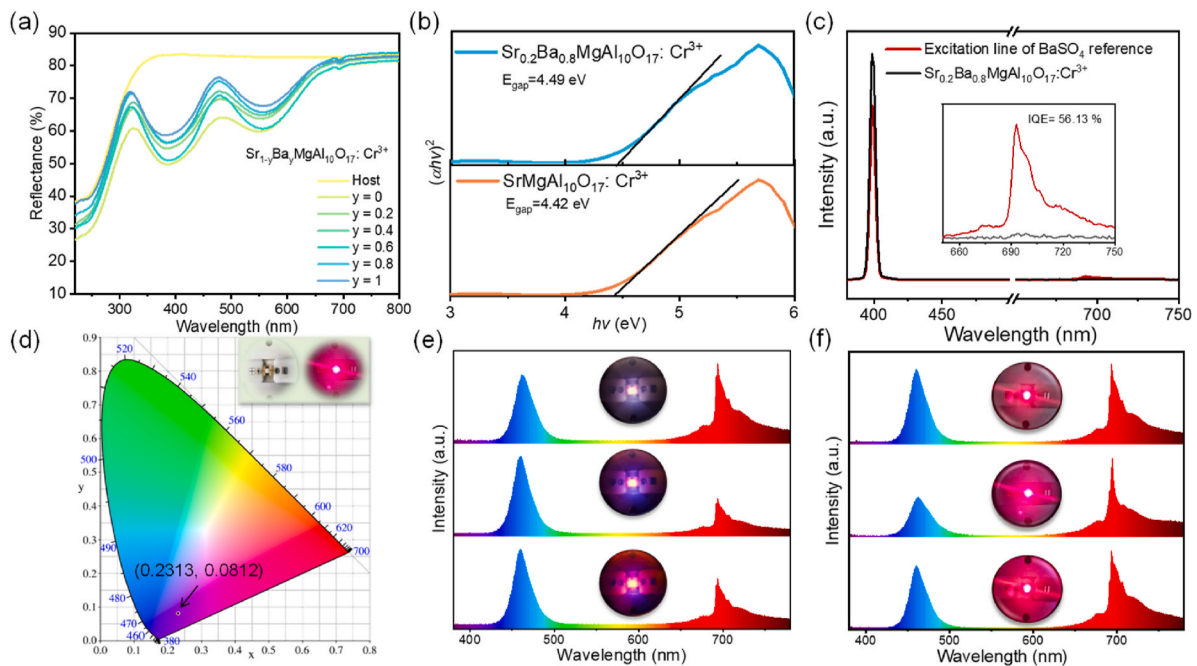


Fig. 5. (a) UV diffuse reflectance spectra of  $\text{Sr}_{1-y}\text{Ba}_y\text{MgAl}_{10}\text{O}_{17}:\text{Cr}^{3+}$  ( $y = 0-1$ ) and host; (b) Optical band gap calculation of  $\text{SrMgAl}_{10}\text{O}_{17}:\text{Cr}^{3+}$  and  $\text{Sr}_{0.8}\text{Ba}_{0.2}\text{MgAl}_{10}\text{O}_{17}:\text{Cr}^{3+}$ ; (c) The quantum yield of  $\text{Sr}_{0.2}\text{Ba}_{0.8}\text{MgAl}_{10}\text{O}_{17}:\text{Cr}^{3+}$ ; (d) CIE coordinate chart of  $\text{Sr}_{0.8}\text{Ba}_{0.2}\text{MgAl}_{10}\text{O}_{17}:\text{Cr}^{3+}$ ; (e) and (f) Electroluminescence spectra of  $\text{Sr}_{1-y}\text{Ba}_y\text{MgAl}_{10}\text{O}_{17}:\text{Cr}^{3+}$  ( $y = 0-1$ ).

$$(ah\nu)^n = (h\nu - E_g) \quad (6)$$

where  $h\nu$  is the photon energy and  $\alpha$  represents the absorption coefficient, based on the reported  $\text{SrMgAl}_{10}\text{O}_{17}:\text{Cr}^{3+}$  belongs to the direct bandgap structure, so  $n$  is 2. The intercept marked in the corresponding Fig. 5b is the optical band gap of the material. The optical band gap of  $\text{SrMgAl}_{10}\text{O}_{17}:\text{Cr}^{3+}$  and  $\text{Sr}_{0.2}\text{Ba}_{0.8}\text{MgAl}_{10}\text{O}_{17}:\text{Cr}^{3+}$  was calculated to be 4.42 eV and 4.49 eV, respectively, and the size of the optical band gap could correspond to the thermal stability of the material to some extent.

An important indicator to evaluate the performance of phosphors is the QE (Fig. 5c), which is calculated by the following equation [45]:

$$\eta = \frac{\int L_s}{\int E_R - \int E_s} \quad (7)$$

where,  $\eta$  is IQE, emission spectra and excitation spectra are represented as  $L_s$ ,  $E_s$  is  $\text{BaSO}_4$  reference excitation line  $E_R$ , and sample excitation spectra. An excitation wavelength of 399 nm and emission range of 660 nm–750 nm were used to test the QE. The IQE of  $\text{SrMgAl}_{10}\text{O}_{17}:\text{Cr}^{3+}$  is 36.15% and the IQE of  $\text{Sr}_{0.2}\text{Ba}_{0.8}\text{MgAl}_{10}\text{O}_{17}:\text{Cr}^{3+}$  phosphor is 56.13% (Fig. S4). This is higher than previously reported and has the potential applications of plant growth LEDs [46].

To verify the potential application of  $\text{Sr}_{0.2}\text{Ba}_{0.8}\text{MgAl}_{10}\text{O}_{17}:\text{Cr}^{3+}$  phosphor in plant growth, it was packaged as an LED device using a 470 nm blue chip. Fig. 5d shows the Commission Internationale de l'Éclairage (CIE) chromaticity coordinate of (0.2313, 0.0812) for the electroluminescence characteristics of the devices. The inset is the physical picture of the prepared LED devices. Fig. 5e and f and its illustrations reveal the EL spectra and photographs of the luminescence of these fabricated LED devices. The comparison between the electroluminescence spectrum and the plant pigment absorption spectrum is shown in Fig. 6. The prepared device can well match the phytochrome PFR in the range of 650–780 nm, which represents the application potential of the material.

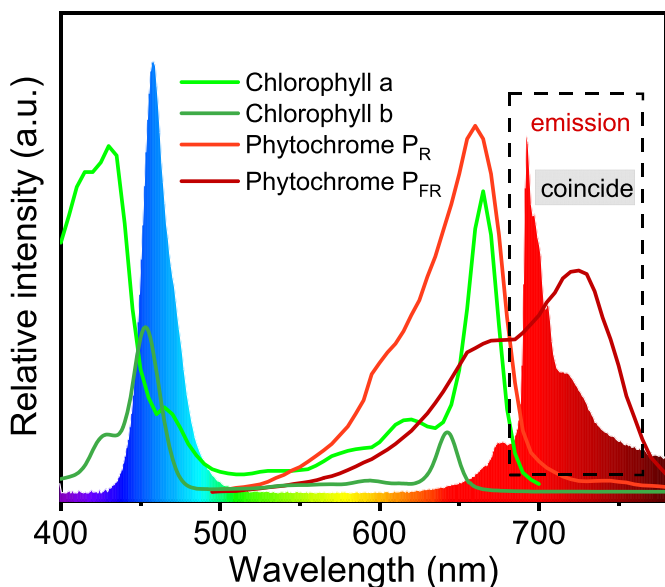


Fig. 6. Matching of the prepared devices to plant pigments.

#### 4. Conclusion

In summary, a series of  $\text{SrMgAl}_{10}\text{O}_{17}: x\text{Cr}^{3+}$  and its solid solution phosphors were prepared by the high-temperature solid phase method, and XRD and Rietveld refinement confirmed the pure phase of the materials. The change in luminescence performance was recorded during the process of gradually replacing  $\text{Sr}^{2+}$  ion with  $\text{Ba}^{2+}$  ion and gradually changing from  $[\text{SrO}_6]$  to  $[\text{BaO}_6]$ . Specifically, the  ${}^2\text{E} \rightarrow {}^4\text{A}_2$  dominated far-red light emission of  $\text{Cr}^{3+}$  in  $\text{SrMgAl}_{10}\text{O}_{17}$  is enhanced due to the gradual increase in crystal field strength. Specifically, it is the strongest at  $y = 0.8$ , reaching 254 % of the initial value. The IQE of the  $\text{Ba}^{2+}$  ion substituted phosphor reached 56.13%, which is higher than that reported previously, indicating the good performance of the material. The far-red light emission at 693 nm can well correspond to the plant phytochrome  $\text{P}_{\text{FR}}$ , which represents the material that has great application prospects in the field of plant lighting.

#### CRediT authorship contribution statement

**Yibiao Ma:** Writing – review & editing, Writing – original draft, Investigation. **Weifang Liao:** Data curation. **Beibei Quan:** Data curation. **Zihui Kong:** Data curation. **Maxim S. Molochev:** Software, Data curation. **Andrey Zolotov:** Data curation. **Ming Cheng:** Funding acquisition. **Xiaoyan Chen:** Funding acquisition. **Zhi Zhou:** Investigation, Formal analysis. **Mao Xia:** Methodology.

#### Declaration of competing interest

The authors declare that they have no known competing financial interests or personal relationships that could have appeared to influence the work reported in this paper.

#### Data availability

Data will be made available on request.

#### Acknowledgments

The authors would like to gratefully acknowledge funds from the Key R & D Projects in Hunan Province (2021SK2047, 2022NK2044), the Wangcheng Science and Technology Plan (KJ221017), the Science and Technology Innovation Program of Hunan Province (2022WZ1022).

The work was supported by the Ministry of Science and Higher Education of the Russian Federation as part of the World-class Research Center program: “Advanced Digital Technologies”, contract no. 075-15-2020-935. Research Foundation of Education Bureau of Hunan Province, China (22B0211).

#### Appendix A. Supplementary data

Supplementary data to this article can be found online at <https://doi.org/10.1016/j.jlumin.2024.120553>.

#### References

- [1] P.X. Gao, P. Dong, Z.Y. Zhou, Q. Li, H.H. Li, Z. Zhou, M. Xia, P.H. Zhang, Enhanced luminescence and energy transfer performance of double perovskite structure  $\text{Gd}_2\text{MgTiO}_6:\text{Bi}^{3+}, \text{Mn}^{4+}$  phosphor for indoor plant growth LED lighting, *Ceram. Int.* 47 (2021) 16588–16596.
- [2] E. Appolloni, G. Pennisi, I. Zauli, L. Carotti, I. Paucek, S. Quaini, F. Orsini, G. Gianquinto, Beyond vegetables: effects of indoor LED light on specialized metabolite biosynthesis in medicinal and aromatic plants, edible flowers, and microgreens, *J. Sci. Food Agric.* 102 (2022) 472–487.
- [3] N. Budhlakoti, A.K. Kushwaha, A. Rai, K.K. Chaturvedi, A. Kumar, A.K. Pradhan, U. Kumar, R.R. Kumar, P. Juliana, D.C. Mishra, S. Kumar, Genomic selection: a tool for accelerating the efficiency of molecular breeding for development of climate-resilient crops, *Front. Genet.* 13 (2022) 832153.
- [4] F. Sheibani, M. Bourget, R.C. Morrow, C.A. Mitchell, Close-canopy lighting, an effective energy-saving strategy for overhead sole-source LED lighting in indoor farming, *Front. Plant Sci.* 14 (2023).
- [5] K. Deng, Y. Jin, L. Yuan, B. Wang, H. Wu, Y. Hu, A thermal-stable  $\text{Mn}^{4+}$ -doped far-red-emitting phosphor-converted LED for indoor plant cultivation, *Mater. Today Chem.* 26 (2022) 101010.
- [6] C.A. Mitchell, History of controlled environment horticulture: indoor farming and its Key Technologies, *Hortscience* 57 (2022) 247–256.
- [7] X. Qin, X.W. Liu, W. Huang, M. Bettinelli, X.G. Liu, Lanthanide-activated phosphors based on 4f-5d optical transitions: theoretical and experimental aspects, *Chem. Rev.* 117 (2017) 4488–4527.
- [8] G. Samuoliene, G. Sabajeviene, A. Urbonaviciute, P.J.A.B.S. Duchovskis, Carrot lowering initiation: light effect, photosynthetic pigments, carbohydrates, *J. Photochem. Photobiol. B* 51, 2007, pp. 39–42.
- [9] T.T. Tan, S.L. Li, Y.F. Fan, Z.L. Wang, M.A. Raza, I. Shafiq, B.B. Wang, X.L. Wu, T. W. Yong, X.C. Wang, Y.S. Wu, F. Yang, W.Y. Yang, Far-red light: a regulator of plant morphology and photosynthetic capacity, *Crop J.* 10 (2022) 300–309.
- [10] J. Lanoue, C. Little, X.M. Hao, The power of far-red light at night: photomorphogenic, physiological, and yield response in pepper during dynamic 24 hour lighting, *Front. Plant Sci.* 13 (2022) 857616.
- [11] X.J. Kang, W. Lü, Z.N. Zhu, C.Y. Jia, A novel blue-light excitable  $\text{Pr}^{3+}$ -doped (Sr,Ba)  $\text{LaMgTaO}_6$  phosphor for plant growth lighting, *J. Rare Earths* 41 (2023) 666–672.
- [12] Q. Sun, S. Wang, B. Li, H. Guo, X. Huang, Synthesis and photoluminescence properties of deep red-emitting  $\text{CaGdAlO}_4: \text{Mn}^{4+}$  phosphors for plant growth LEDs, *J. Lumin.* 203 (2018) 371–375.
- [13] H. Yu, J. Chan, B. Devakumar, X. Huang, Highly efficient far-red emitting  $\text{Mn}^{4+}$ -activated  $\text{Li}_3\text{La}_3\text{W}_2\text{O}_{12}$  phosphors for plant growth LED lighting, *Mater. Today Chem.* 30 (2023) 101584.
- [14] X.Y. Huang, H. Guo, Finding a novel highly efficient  $\text{Mn}^{4+}$ -activated  $\text{Ca}_3\text{La}_2\text{W}_2\text{O}_{12}$  far-red emitting phosphor with excellent responsiveness to phytochrome  $\text{P}_{\text{FR}}$ : towards indoor plant cultivation application, *Dyes Pigments* 152 (2018) 36–42.
- [15] N. Yeh, J.P. Chung, High-brightness LEDs—energy efficient lighting sources and their potential in indoor plant cultivation, *Renew. Sustain. Energy Rev.* 13 (2009) 2175–2180.
- [16] K.M. Zielinska-Dabkowska, J. Hartmann, C. Sigillo, LED light sources and their complex set-up for visually and biologically effective illumination for ornamental indoor plants, *Sustainability* 11 (2019) 2642.
- [17] N.Z. Khan, S.A. Khan, A. Jalil, F. Wang, I. Mehmood, M.T. Abbas, L. Ali, M. Sohail, X. Xu, S. Agathopoulos, Structural development and luminescent enhancement of  $\text{CaAlSi}_3\text{N}_3:\text{Eu}^{2+}$  phosphor via replacing  $\text{Al}^{3+}$  by  $\text{Ga}^{3+}$ , *J. Alloys Compd.* 897 (2022) 162485.
- [18] K. Uheda, N. Hirosaki, Y. Yamamoto, A. Naito, T. Nakajima, H. Yamamoto, Luminescence properties of a red phosphor,  $\text{CaAlSi}_3\text{N}_3: \text{Eu}^{2+}$ , for white light-emitting diodes, *Electrochem. Solid State Lett.* 9 (2006) H22.
- [19] Y. Zhang, Z. Zhang, X. Liu, G. Shao, L. Shen, J. Liu, W. Xiang, X. Liang, A high quantum efficiency  $\text{CaAlSi}_3\text{N}_3: \text{Eu}^{2+}$  phosphor-in-glass with excellent optical performance for white light-emitting diodes and blue laser diodes, *Chem. Eng. J.* 401 (2020) 125983.
- [20] J.D. Majher, M.B. Gray, T.A. Strom, P.M. Woodward,  $\text{Cs}_2\text{NaBiCl}_6: \text{Mn}^{2+}$ —a new orange-red halide double perovskite phosphor, *Chem. Mater.* 31 (2019) 1738–1744.
- [21] C. Zhou, L. Peng, Z. Kong, M. Wu, M.S. Molochev, Z. Zhou, J. Wang, M. Xia, A high thermal stability  $\text{Cr}^{3+}$ -doped gallate far red phosphor for plant lighting: structure, luminescence enhancement and application prospect, *J. Mater. Chem. C* 10 (2022) 5829–5839.

- [22] S. Zhang, Y. Liu, J. Yin, X. Zhang, Y. Li, L. Su, Z. Zhou, M. Xia, A novel Cr<sup>3+</sup>-activated far-red titanate phosphor: synthesis, luminescence enhancement and application prospect, *Mater. Today Chem.* 24 (2022) 100835.
- [23] Y. Ma, S. Li, J. Wei, W. Liao, B. Quan, M.S. Molokeev, M. Cheng, X. Chen, Z. Zhou, M. Xia, Spectroscopically enhanced far-red phosphor Li<sub>2</sub>Mg<sub>3</sub>TiO<sub>6</sub>: Cr<sup>3+</sup> and its application prospects to the cold resistance of rice, *Mater. Adv.* 4 (2023) 5808–5816.
- [24] G. Liu, Z. Xia, Modulation of thermally stable photoluminescence in Cr<sup>3+</sup>-based near-infrared phosphors, *J. Phys. Chem. Lett.* 13 (2022) 5001–5008.
- [25] G. Sridhar, D. Hebbar, S.G. Menon, P.M. Lewis, K. Choudhari, R.E. Kroon, H. C. Swart, S.D. Kulkarni, Cr-doped ZnGa<sub>2</sub>O<sub>4</sub>: simple synthesis of intense red-NIR emitting nanoparticles with enhanced quantum efficiency, *Opt. Mater.* 123 (2022) 111919.
- [26] C. Lee, Y. Liu, B. Hulme, L.Y. Chang, S.W. Ke, E.R. Wang, Y.H. Wu, B.H. Lin, Y. Jiang, L. Liu, ZnGa<sub>2</sub>O<sub>4</sub>: Cr<sup>3+</sup>@ calcium phosphate nanocomposite with near-infrared persistent luminescence and high stability, *ChemPhotoChem* 7 (2023) e202300143.
- [27] P. Xiong, B. Huang, D. Peng, B. Viana, M. Peng, Z. Ma, Self-recoverable mechanically induced instant luminescence from Cr<sup>3+</sup>-doped LiGa<sub>5</sub>O<sub>8</sub>, *Adv. Funct. Mater.* 31 (2021) 2010685.
- [28] G. Liu, M.S. Molokeev, Z. Xia, Structural rigidity control toward Cr<sup>3+</sup>-based broadband near-infrared luminescence with enhanced thermal stability, *Chem. Mater.* 34 (2022) 1376–1384.
- [29] S. Motloung, F. Dejene, H. Swart, O. Ntwaeaborwa, Effects of Cr<sup>3+</sup> mol% on the structure and optical properties of the ZnAl<sub>2</sub>O<sub>4</sub>: Cr<sup>3+</sup> nanocrystals synthesized using sol-gel process, *Ceram. Int.* 41 (2015) 6776–6783.
- [30] M.T. Tran, D.Q. Trung, N. Tu, D.D. Anh, L.T.H. Thu, N.V. Du, N.V. Quang, N. T. Huyen, N.D.T. Kien, D.X. Viet, N.D. Hung, P.T. Huy, Single-phase far-red-emitting ZnAl<sub>2</sub>O<sub>4</sub>:Cr<sup>3+</sup> phosphor for application in plant growth LEDs, *J. Alloys Compd.* 884 (2021) 161077.
- [31] H. Tanno, S. Zhang, T. Shinoda, H. Kajiyama, Characteristics of photoluminescence, thermoluminescence and thermal degradation in Eu-doped BaMgAl<sub>10</sub>O<sub>17</sub> and SrMgAl<sub>10</sub>O<sub>17</sub>, *J. Lumin.* 130 (2010) 82–86.
- [32] H. Kang, K.N. Lee, S. Unithrattil, H.J. Kim, J.H. Oh, J.S. Yoo, W.B. Im, Y.R. Do, Narrow-band SrMgAl<sub>10</sub>O<sub>17</sub>:Eu<sup>2+</sup>, Mn<sup>2+</sup> green phosphors for wide-color-gamut backlight for LCD displays, *ACS Omega* 5 (2020) 19516–19524.
- [33] T. Wanjun, C. Donghua, W. Ming, Luminescence studies on SrMgAl<sub>10</sub>O<sub>17</sub>: Eu, Dy phosphor crystals, *Opt Laser. Technol.* 41 (2009) 81–84.
- [34] S. Adachi, Luminescence spectroscopy of Cr<sup>3+</sup> in an oxide: a strong or weak crystal-field phosphor, *J. Lumin.* 234 (2021) 117965.
- [35] J. Li, H. Zhe, H. Ming, Y. Zhou, Y. Ye, Q. Zhou, Z. Wang, A near-infrared phosphor doped with Cr<sup>3+</sup> towards zero-thermal-quenching for high-power LEDs, *Mater. Today Chem.* 24 (2022) 100839.
- [36] H. Xiao, J. Zhang, L. Zhang, H. Wu, H. Wu, G. Pan, F. Liu, J. Zhang, Cr<sup>3+</sup> activated garnet phosphor with efficient blue to far-red conversion for pc-LED, *Adv. Opt. Mater.* 9 (2021) 2101134.
- [37] L. You, R. Tian, T. Zhou, R.-J. Xie, Broadband near-infrared phosphor BaMgAl<sub>10</sub>O<sub>17</sub>:Cr<sup>3+</sup> realized by crystallographic site engineering, *Chem. Eng. J.* 417 (2021) 129224.
- [38] M. Back, E. Trave, J. Ueda, S. Tanabe, Radiometric optical thermometer based on dual near-infrared emission in Cr<sup>3+</sup>-doped bismuth-based gallate host, *Chem. Mater.* 28 (2016) 8347–8356.
- [39] Y. Wang, Z. Wang, G. Wei, Y. Yang, S. He, J. Li, Y. Shi, R. Li, J. Zhang, P. Li, Highly efficient and stable near-infrared broadband garnet phosphor for multifunctional phosphor-converted light-emitting diodes, *Adv. Opt. Mater.* 10 (2022) 2200415.
- [40] Y. Zhou, H. Xiang, Al<sub>5</sub>BO<sub>9</sub>: a wide band gap, damage-tolerant, and thermal insulating lightweight material for high-temperature applications, *J. Am. Ceram. Soc.* 99 (2016) 2742–2751.
- [41] C. Struck, W.J.J.o.L. Fonger, Unified model of the temperature quenching of narrow-line and broad-band emissions 10 (1975) 1–30.
- [42] C. Struck, W. Fonger, Unified model of the temperature quenching of narrow-line and broad-band emissions, *J. Lumin.* 10 (1975) 1–30.
- [43] K. Munirathnam, K. Mallikarjuna, R. Vijaya, P.C. Nagajyothi, K.R. Reddy, M. Srinivas, Spectral change and far-red emission of Mn<sup>2+</sup> ions co-doped NaSrB<sub>5</sub>O<sub>9</sub>: Dy<sup>3+</sup> luminescence material for plant growth LEDs, *J. Rare Earths* 40 (2022) 218–225.
- [44] M. Zhang, Z. Wang, X. Wang, H. Suo, L. Cao, Y. Yao, M. Zheng, J. Cui, Z. Yang, P. Li, Competitive Cr<sup>3+</sup> occupation in persistent phosphors toward tunable traps distribution for dynamic anti-counterfeiting, *J. Am. Ceram. Soc.* 104 (2021) 5224–5234.
- [45] J. Zhang, J. Zhang, W. Zhou, X. Ji, W. Ma, Z. Qiu, L. Yu, C. Li, Z. Xia, Z. Wang, Composition screening in blue-emitting Li<sub>4</sub>Sr<sub>1+x</sub>Ca<sub>0.97-x</sub>(SiO<sub>4</sub>)<sub>2</sub>: Ce<sup>3+</sup> phosphors for high quantum efficiency and thermally stable photoluminescence, *ACS Appl. Mater. Interfaces* 9 (2017) 30746–30754.
- [46] Y.J. Han, L. Shi, H. Liu, Z.W. Zhang, A novel far red-emitting phosphor SrMgAl<sub>10</sub>O<sub>17</sub>: Cr<sup>3+</sup> for warm w-LEDs, *Optik* 195 (2019) 162014.